Reactions of Atomic Silicon and Germanium with Ammonia: A Matrix-Isolation FTIR and Theoretical Study

Mohua Chen, Aihua Zheng, Hao Lu, and Mingfei Zhou*

Department of Chemistry and Laser Chemistry Institute, Fudan University, Shanghai 200433, P. R. China

Received: July 30, 2001; In Final Form: January 14, 2002

The reactions of Si atoms with NH_3 molecules have been studied using matrix-isolation FTIR spectroscopy and density functional theoretical calculations. Silicon atoms reacted with NH_3 to form the $SiNH_3$ complex spontaneously in solid argon upon annealing. Mercury arc photolysis with a 290-nm long-wavelength pass filter destroyed the $SiNH_3$ absorptions and produced $HSiNH_2$ absorptions. Full-arc irradiation (250−580 nm) destroyed the $HSiNH_2$ absorptions and produced SiNH absorptions. The potential energy surface along the reaction path leading to the observed products has also been calculated. Similar experiments with Ge gave spectra for the analogous product molecules.

1. Introduction

Interest in the study of the surface chemistry of silicon has been enhanced over the past few decades. The silicon surface is the most commonly used surface in device manufacture because of its anisotropic etching properties. Nitridation of silicon surface creates silicon nitride films, which are widely used in integrated circuits as insulating and passivating layers. NH_3 is an excellent nitriding agent for the production of ultrathin silicon nitride interfaces which are necessary for the next generation of very large integrated devices.[1] The experimental and theoretical modeling of the surface reactions at the atomic−molecular level is particularly helpful in providing better insight into the mechanism of surface reactions, in which reactive intermediates might be involved. The interaction of ammonia with bulk silicon surfaces or silicon clusters has been the subject of many experimental and theoretical studies.[2−4] To our knowledge, there have been no reports on the reactions of atomic Si with ammonia molecules.

Matrix-isolation spectroscopic methods have been widely used to investigate the reactions of transition metal atoms, as well as main group atoms, with small molecules such as H_2,[5] O_2,[6] H_2O,[7] and NH_3.[8] In solid matrixes, Fe, Ni, and Cu atoms formed adduct with one or two NH_3 molecules,[9−11] and UV irradiation induced the insertion of the metal into a N−H bond with the formation of the amido derivatives $HMNH_2$ (M = Fe, Ni, and Cu), $HMNH_2NH_3$ (M = Fe or Ni), and H + MNH_2 (M = Cu). The reactions between group IIIA atoms and ammonia in solid matrixes have been studied by several groups. An EPR study revealed the formation of $Al(NH_3)_2$ and $Al(NH_3)_4$ adducts.[12] Andrews and co-workers reported that electronically excited Al atoms reacted with ammonia to form the $HAlNH_2$ and $AlNH_2$ molecules.[13] Recently, the thermal and photochemical reactions of the group IIIA metals Al, Ga, and In with ammonia have been investigated by Himmel et al., who characterized the MNH_3, $HMNH_2$, MH_2, and H_2MNH_2 species that were generated.[14]

In this paper, we report a combined matrix-isolation FTIR spectroscopic and theoretical study of the reactions of Si atoms with NH_3 molecules in solid argon. Recent studies in our laboratory have shown that the combination of matrix-isolation FTIR and density functional theoretical calculations has been extremely beneficial in understanding and interpreting reaction mechanisms.[15−17] Although this study seems parallel to that of NH_3 with group 13 metal atoms, we will show that the chemistry is distinctly different because of the intrinsic difference between Si and group 13 metals. We will show that ground-state silicon atoms form a complex with ammonia spontaneously in solid argon. The complex undergoes photon-induced rearrangement to form the insertion intermediate $HSiNH_2$, which decomposes to SiNH upon full-arc mercury lamp irradiation.

Particularly relevant to present study is the previous generation and spectroscopic identification of $HSiNH_2$, H_2SiNH, SiNH, and HSiN by the photon-induced decomposition of precursor molecules in solid matrixes.[18−20] The geometries, relative stabilities, and reactivities of these silicon−nitrogen containing species have also been the subject of several theoretical studies.[21−23]

2. Experimental and Theoretical Methods

The technique used for pulsed laser ablation and matrix-isolation infrared spectroscopic investigation has been described in detail previously.[24] The 1064-nm fundamental of a Nd:YAG laser (Spectra Physics, DCR 2, 20-Hz repetition rate and 8-ns pulse width) was focused onto a rotating silicon or germanium target through a hole in a CsI window. Typically, 5−10 mJ/pulse of laser power was used. The ablated Si or Ge atoms were codeposited with molecular NH_3 in excess argon onto an 11-K CsI window at a rate of 2−4 mmol/h. The CsI window was mounted on a copper holder at the cold end of a cryostat (Air Products Displex DE 202), and the temperature was maintained by a closed-cycle helium refrigerator (Air Products Displex 1R02W). FTIR spectra were recorded on a Bruker IFS 113v Fourier transform infrared spectrometer equipped with a DTGS detector with a resolution of 0.5 cm^{-1}. Isotopic $^{15}NH_3$ was prepared by the thermal dissociation of $(^{15}NH_4)_2SO_4$ (98%). Matrix samples were annealed at different temperatures and subjected to photolyses at different wavelengths using a high-pressure mercury lamp (250-W, without globe) and glass filters.

* Corresponding author. E-mail: mfzhou@fudan.edu.cn. Fax: +86-21-65643532.

10.1021/jp012928z CCC: $22.00
Published on Web 03/07/2002

TABLE 1: Infrared Absorptions (cm^{-1}) following the Reaction of Si Atoms with NH_3 Molecules in an Argon Matrix

$Si + {}^{14}NH_3$	$Si + {}^{15}NH_3$	annealing[a]	$\lambda > 290$ nm[a]	$\lambda > 250$ nm[a]	assignment[b]
3570.8	3561.3			↑	SiNH, ν(N−H)
3387.1	3378.7	↑	↓		$SiNH_3$, ν^{asym}(N−H)
1927.0	1926.7		↑	↓	$HSiNH_2$, ν(H−Si)
1599.3	1596.0	↑	↓		$SiNH_3$, $\delta^{asym}(NH_3)$
1196.9	1173.2			↑	SiNH, ν(Si−N)
1185.5	1180.0	↑	↓		$SiNH_3$, $\delta^{sym}(NH_3)$
938.6	934.3		↑	↓	$HSiNH_2$, $\beta(NH_2)$
853.8	838.0		↑	↓	$HSiNH_2$, ν(Si−N)
562.8	559.2		↑	↓	$HSiNH_2$, $\omega(NH_2)$
514.9	512.3			↑	SiNH, δ(SiNH)
510.0	507.5			↑	SiNH, site

[a] ↑, increase; ↓, decrease. [b] ν, stretching mode; δ, bending; β, wagging; ω, out-of-plane rocking.

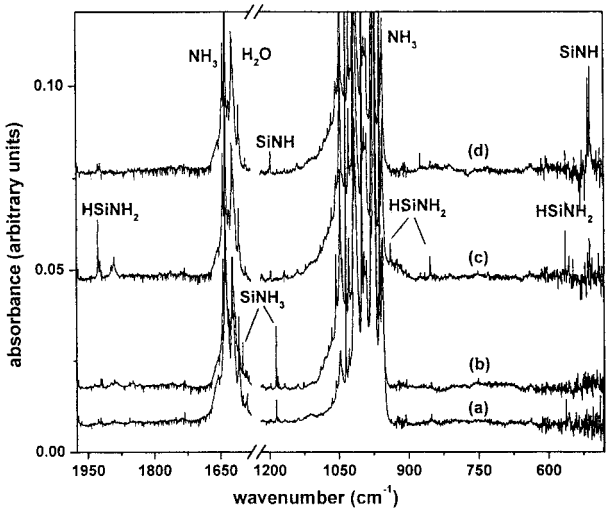

Figure 1. Infrared spectra in the 1975−1580 and 1220−480 cm^{-1} regions following the codeposition of laser-ablated Si atoms with 0.2% NH_3 in argon: (a) as-deposited at 11 K, (b) after 25-K annealing, (c) after 20 min of $\lambda > 290$ nm photolysis, and (d) after 20 min of $\lambda > 250$ nm photolysis.

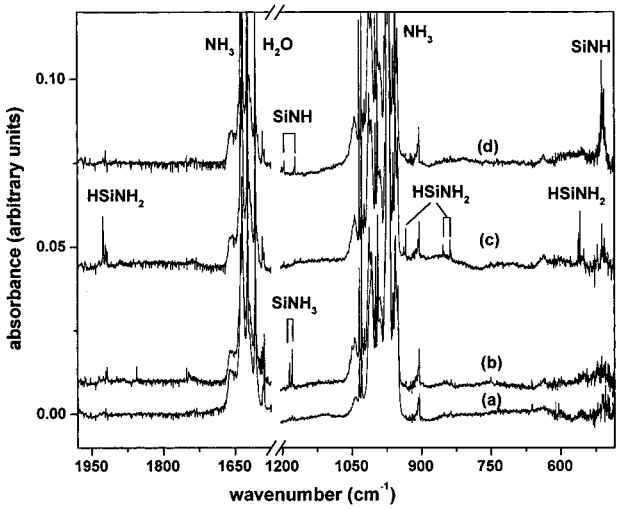

Figure 2. Infrared spectra in the 1980−1575 and 1205−485 cm^{-1} regions following the codeposition of laser-ablated Si atoms with 0.1% $^{14}NH_3$ + 0.2% $^{15}NH_3$ in argon: (a) as-deposited at 11 K, (b) after 25-K annealing, (c) after 20 min of $\lambda > 290$ nm photolysis, and (d) after 20 min of $\lambda > 250$ nm photolysis.

Density functional calculations were performed using the Gaussian 98 program.[25] The three-parameter hybrid functional of Becke with additional correlation corrections due to Lee, Yang, and Parr (B3LYP)[26,27] and the 6-311++G(d,p) basis set were used.[28,29] The geometries of products were fully optimized and vibrational frequencies were calculated with analytic second derivatives. Transition state optimizations were done with the synchronous transit-guided quasi-Newton (STQN) method,[30] followed by vibrational frequency calculations showing the obtained structures to be true saddle points.

3. Results

FTIR spectra of the Si + NH_3/Ar and Ge + NH_3/Ar systems and DFT calculation results are presented in this section.

Si + NH_3/Ar. Representative spectra in selected regions from the co-condensation of laser-ablated Si atoms with 0.2% NH_3 in argon are shown in Figure 1, and the infrared absorptions are summarized in Table 1. One-hour sample deposition at 11 K resulted in strong NH_3 and weak $(NH_3)_n$ ($n > 1$), H_2O, and $NH_3 \cdot H_2O$ absorptions.[31,32] Three new absorptions at 3387.1, 1599.3, and 1185.5 cm^{-1} were also observed after sample deposition and increased together markedly upon annealing. Upon subsequent high-pressure mercury lamp photolysis with a 290-nm long-wavelength pass filter, the absorptions at 3387.1, 1599.3, and 1185.5 cm^{-1} were destroyed, and new absorptions at 1927.0, 1557.8, 938.6, 853.8, and 562.8 cm^{-1} were produced. Upon further full-arc photolysis, the 1927.0, 1557.8, 938.6, 853.8, and 562.8 cm^{-1} absorptions disappeared with the simultaneous growth of a set of bands at 3570.8, 1196.9, and 514.9 cm^{-1} (with a site band at 510.0 cm^{-1}).

N-15 isotopic substitution was employed for band identification, with the results included in Table 1. All of the new product absorptions underwent substantial shifts in the experiment employing $^{15}NH_3$. Figure 2 shows the mixed $^{14}NH_3$ + $^{15}NH_3$ spectra in selected regions.

Ge + NH_3. Similar experiments were also performed for Ge + NH_3 reaction. The IR absorption spectra in selected regions are presented in Figure 3, with the absorptions listed in Table 2. In addition to the absorptions due to NH_3, $(NH_3)_x$, H_2O, and $NH_3 \cdot H_2O$, new features at 1578.4 and 1128.7 cm^{-1} appeared upon sample deposition and markedly increased upon annealing. These two bands disappeared upon high-pressure mercury lamp photolysis with a 290-nm long-wavelength pass filter, while a set of new absorptions at 1793.3, 863.2, 692.8, and 474.0 cm^{-1} was developed. Subsequent full-arc photolysis almost destroyed these bands. The spectra for a $^{15}NH_3$/Ar sample are shown in Figure 4. All of the new product absorptions exhibited isotopic shifts, as listed in Table 2.

Calculation Results. B3LYP/6-311++G(d,p) calculations were done on three MNH_3 isomers (M = Si, Ge), namely, the MNH_3 complex and the inserted $HMNH_2$ and H_2MNH molecules in both singlet and triplet states. The optimized geometric parameters are shown in Figure 5 (the parameters of Ge-containing species are given in parentheses), and the vibrational frequencies and intensities are listed in Tables 3 and 4. The

TABLE 2: Infrared Absorptions (cm^{-1}) following the Reaction of Ge Atoms and NH_3 Molecules in an Argon Matrix

$Ge + {}^{14}NH_3$	$Ge + {}^{15}NH_3$	annealing[a]	$\lambda > 290$ nm[a]	$\lambda > 250$ nm[a]	assignment[b]
1793.3	1793.2		↑	↓	$HGeNH_2$, ν(H−Ge)
1787.9	1787.7		↑	↓	$HGeNH_2$, site
1578.4		↑	↓		$GeNH_3$, $\delta^{asym}(NH_3)$
1128.7	1123.2	↑	↓		$GeNH_3$, $\delta^{sym}(NH_3)$
1125.1	1119.8	↑	↓		$GeNH_3$, site
863.2	859.3		↑	↓	$HGeNH_2$, $\beta(NH_2)$
692.8	678.4		↑	↓	$HGeNH_2$, ν(Ge−N)
474.0	471.3		↑	↓	$HGeNH_2$, $\omega(NH_2)$
460.3	457.3		↑	↓	$HGeNH_2$, site

[a] ↑, increase; ↓, decrease. [b] ν, stretching mode; δ, bending; β, wagging; ω, out-of-plane rocking.

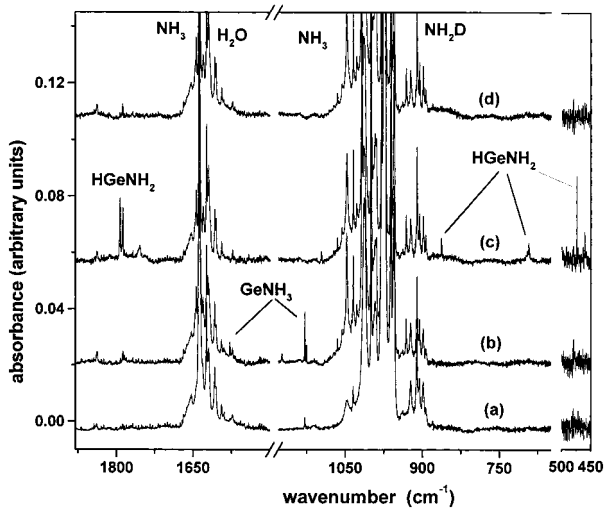

Figure 3. Infrared spectra in the 1880−1500, 1180−650 and 500−450 cm^{-1} regions following the codeposition of laser-ablated Ge atoms with 0.2% NH_3 in argon: (a) as-deposited at 11 K, (b) after 25-K annealing, (c) after 20 min of $\lambda > 290$ nm photolysis, and (d) after 20 min of $\lambda > 250$ nm photolysis.

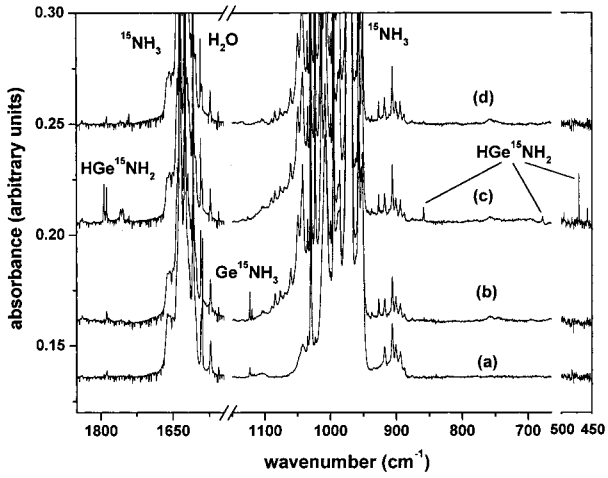

Figure 4. Infrared spectra in the 1850−1545, 1150−665 and 500−450 cm^{-1} regions following the codeposition of laser-ablated Ge atoms with 0.2% $^{15}NH_3$ in argon: (a) as-deposited at 11 K, (b) after 25-K annealing, (c) after 20 min of $\lambda > 290$ nm photolysis, and (d) after 20 min of $\lambda > 250$ nm photolysis.

$SiNH_3$ and $GeNH_3$ complexes were predicted to have $^3A_1$ ground states with C_{3v} symmetry. Both the $HMNH_2$ and H_2MNH (M = Si and Ge) isomers were calculated to have $^1A'$ ground states with planar structures.

Calculations were also performed on the MNH and HMN (M = Si, Ge) isomers. The optimized structures are also shown in Figure 5, with the vibrational frequencies and intensities summarized in Tables 3 and 4.

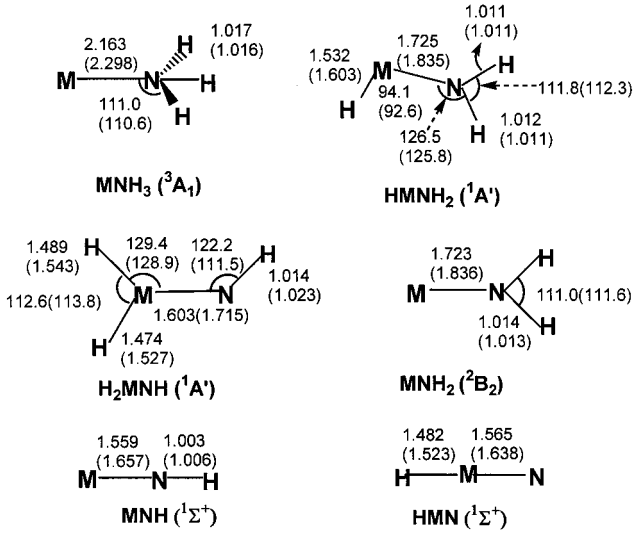

Figure 5. Calculated geometric parameters (bond lengths in angstroms, bond angles in degrees) of the MNH_3, $HMNH_2$, H_2MNH, MNH, and NMH (M = Si and Ge) molecules. Values for Ge compounds are listed in parentheses.

4. Discussion

The product absorptions were assigned by consideration of the frequencies and isotopic shifts of the observed bands and by comparisons with DFT frequency calculations. We then focused on the reaction mechanisms and the potential energy surfaces of the corresponding M + NH_3 reactions (M denotes Si or Ge).

$SiNH_3$. According to the annealing and photolysis behavior at different temperatures, the bands at 3387.1, 1599.3, and 1185.5 cm^{-1} belong to different vibrational modes of a common species. In the Si + $^{15}NH_3$ experiment, these three bands shifted to 3378.7, 1596.0, and 1180.0 cm^{-1} and exhibited $^{14}N/^{15}N$ ratios of 1.0024, 1.0019, and 1.0047, respectively. The band positions, relative intensities, and isotopic ratios of these three bands are very close to those of the antisymmetric N−H stretching, antisymmetric, and symmetric NH_3 deformation modes of a free NH_3 molecule in an argon matrix (for NH_3, 3447.3 cm^{-1}/1.0023, 1638.7 cm^{-1}/1.0018, 974.7 cm^{-1}/1.0043), suggesting that these absorptions are due to one or more NH_3 molecules perturbed by Si atoms. In the mixed $^{14}NH_3$ + $^{15}NH_3$ experiment, only pure isotopic counterparts were observed for each mode, indicating that only one NH_3 unit is involved in this molecule. Judging from the experimental conditions, it seems unlikely that more than one Si atom is involved. We note that, under essentially the same experimental conditions, laser-ablated Si reacted with O_2 to form SiO and SiO_2, and no di- or multi-silicon-containing species were produced upon sample deposition or even upon 30-K annealing.[33] Accordingly, we assigned the 3387.1, 1599.3, and 1185.5 cm^{-1} bands to the $SiNH_3$ molecule.

TABLE 3: Calculated Vibrational Frequencies (cm^{-1}) and Intensities (km/mol) of the Products and Transition States in the Si + NH_3 Reaction

species	frequency (intensity, mode)
$SiNH_3$ ($^3A_1$)	3563.8 (67 × 2, e); 3455.2 (13, a_1); 1651.8 (33 × 2, e); 1221.6 (94, a_1); 544.2 (7 × 2, e); 328.6 (37, a_1)
$Si^{15}NH_3$	3553.2 (67 × 2); 3452.3 (12); 1648.8 (33 × 2); 1215.8 (91); 543.0 (7 × 2); 322.8 (36)
$HSiNH_2$ ($^1A'$)	3644.9 (36, a′); 3552.4 (16, a′); 2001.6 (376, a′); 1602.7 (41, a′); 969.2 (118, a′); 844.2 (77, a′); 739.8 (1, a″); 703.6 (2, a′); 601.9 (251, a″)
$HSi^{15}NH_2$	3634.2 (36); 3547.4 (15); 2001.6 (376); 1597.1 (38); 965.0 (118); 828.6 (74); 739.7 (1); 702.8 (2); 597.9 (248)
H_2SiNH ($^1A'$)	3585.3 (23, a′); 2290.4 (74, a′); 2197.5 (115, a′); 1121.2 (50, a′); 1000.1 (55, a′); 769.0 (42, a′); 744.8 (99, a′); 605.1 (60, a″); 570.6 (76, a′)
SiNH ($^1\Sigma^+$)	3743.0 (96, σ); 1230.0 (69, σ); 544.4 (219 × 2, π)
$Si^{15}NH$	3733.0 (92); 1205.3 (67); 541.4 (216 × 2)
NSiH ($^1\Sigma^+$)	3610.8 (4 × 2, e); 3483.7 (2, a_1); 1668.4 (28 × 2, e); 1002.1 (214, a_1)
$SiNH_2$ ($^2B_2$)	3591.7 (44, b); 3511.7 (7, a_1); 1585.6 (30, a_1); 840.6 (88, a_1); 742.8 (14, b_2); 591.5 (252, b_1)
TS1	3589.6 (43); 3477.8 (9); 1603.3 (61); 1520.9 (12); 903.9 (0); 690.7 (191); 643.6 (12); 501.6 (109); 1365.3i (421)
TS2	3559.2 (122); 3315.8 (80); 1735.7(123); 1629.3 (29); 1360.5 (1); 838.8 (167); 624.9 (149); 491.6 (100); 1510.0i (1798)
TS3	3603.4 (33); 1900.4 (125); 1787.0 (119); 1109.6 (1); 992.4 (123); 890.5 (334); 674.2 (111); 585.5 (165); 1805.7i (748)
TS4	3396.8(2); 2025.7(233); 1929.0(77); 1035.3(158); 925.4(33); 848.2(79); 729.1(125); 509.1(13); 1403.0i (522)

TABLE 4: Calculated Vibrational Frequencies (cm^{-1}) and Intensities (km/mol) of the Products and Transition States in the Ge + NH_3 Reaction

species	frequency (intensity, mode)
$GeNH_3$ ($^3A_1$)	3587.9 (56 × 2, e); 3471.8 (15, a_1); 1655.1 (29 × 2, e); 1165.8 (108, a_1); 486.8 (10 × 2, e); 280.0 (22, a_1)
$Ge^{15}NH_3$	3577.9 (56 × 2); 3469.7 (14); 1651.9 (29 × 2); 1159.7 (104); 485.2 (10 × 2); 273.6 (21)
$HGeNH_2$ ($^1A'$)	3662.1 (31, a′); 3555.9 (15, a′); 1853.9 (449, a′); 1578.2 (24, a′); 885.8 (73, a′); 688.5 (2, a″); 681.2 (51, a′); 643.5 (32, a′); 505.0 (245, a″)
$HGe^{15}NH_2$	3651.1 (31); 3551.1 (14); 1853.9 (449); 1572.8 (22); 881.7 (74); 688.4 (2); 669.7 (32); 638.5 (47); 501.7 (243)
GeNH ($^1\Sigma^+$)	3697.6 (85, σ); 989.1 (78, σ); 424.1 (232 × 2, π)
H_2GeNH ($^1A'$)	3474.6 (9, a′); 2185.1 (71, a′); 2085.0 (113, a′); 950.9 (52, a′); 868.5 (55, a′); 865.5 (35, a′); 769.6 (47, a″); 532.5 (44, a′); 503.3 (13, a″)
NGeH ($^1\Sigma^+$)	2113.4 (31, σ); 1037.3 (0, σ); 273.3 (10 × 2, π)
$GeNH_2$ ($^2B_2$)	3621.7 (40, b_2); 3524.4 (9, a_1); 1565.9 (18, a_1); 702.3 (16, b_2); 662.9 (82, a_1); 498.7 (249, b_1)
TS1	3605.0 (36); 3488.5 (13); 1532.3 (55); 1485.6 (68); 845.9 (0); 609.3 (141); 575.3 (18); 392.5 (83); 1150.0i (143)
TS2	3588.1 (89); 3386.2 (23); 1646.4 (69); 1481.5 (46); 1242.5 (12); 719.1 (126); 515.2 (154); 409.8 (100); 1579.3i (1876)
TS3	3536.6 (14); 1868.3 (121); 1697.6 (115); 1102.9 (1); 868.7 (235); 789.2 (57); 752.0 (137); 511.4 (142); 1821.3i (737)
TS4	3367.1 (1); 1934.0 (232); 1801.2 (40); 1009.5 (128); 857.9 (34); 726.9 (40); 703.6 (80); 520.0 (10); 1265.0i (308)

Density functional calculations predicted the $SiNH_3$ molecule to have a $^3A_1$ ground state with C_{3v} symmetry, which correlates to the Si ^3P ground state. The antisymmetric N−H stretching and antisymmetric and symmetric NH_3 deformation modes were calculated to lie at 3563.8, 1651.8, and 1221.6 cm^{-1}, respectively, which required scaling factors of 0.95, 0.97, and 0.97 to fit the observed values. As listed in Table 3, the calculated isotopic frequency shifts are also in good agreement with the experimental values.

$GeNH_3$. Similar bands at 1578.4 and 1128.7 cm^{-1} in the Ge + NH_3/Ar experiments were assigned, respectively, to the antisymmetric and symmetric NH_3 deformation modes of the $GeNH_3$ molecule. DFT calculations on $GeNH_3$ predicted that the molecule has a C_{3v} triplet ground state. The calculated antisymmetric and symmetric NH_3 deformation frequencies, 1655.1 and 1165.8 cm^{-1}, are in quite good agreement with the experimental values. The N−H stretching modes were not observed in our experiments and were possibly masked by other absorptions or too weak to be observed.

$HSiNH_2$. The bands at 1927.0, 1557.8, 938.6, 853.8, and 562.8 cm^{-1} appeared together upon broad-band photolysis (290−580 nm) with the simultaneous disappearance of the $SiNH_3$ absorptions. These bands were assigned to the $HSiNH_2$ molecule. In the $^{15}NH_3$ experiment, these five bands shifted to 1926.7, 1552.6, 934.3, 838.0, and 559.2 cm^{-1}, respectively. The strongest absorption at 1927.0 cm^{-1} is close to the Si−H stretching vibrations of $HSiOCH_3$ (1925 cm^{-1})[34] and HSiOH (1882 cm^{-1})[35] and undergoes little shift upon ^{15}N substitution, indicating that this band might be due to a terminal Si−H stretching vibration. The 853.8 cm^{-1} band exhibited 15.8 cm^{-1} ^{15}N shift and is due to a Si−N stretching mode. The bands at 1557.8, 938.6, and 562.8 cm^{-1} are due to NH_2 scissoring, wagging, and out-of-plane rocking vibrations, respectively.

The $HSiNH_2$ molecule has been previously prepared by 254-nm light irradiation of silyl azide (H_3SiN_3) in solid Ar and identified spectroscopically by Maier and co-workers.[19,20] Six vibrational fundamentals including symmetric and antisymmetric N−H stretching, Si−H stretching, NH_2 scissoring, Si−N stretching, and NH_2 out-of-plane rocking have been assigned, with each mode exhibiting several site splittings. The band positions of the Si−H and Si−N stretching, NH_2 scissoring, and rocking modes in our experiments are lower than the most intense site absorptions reported by Maier et al.[19] This suggests that most of the $HSiNH_2$ molecules trapped in the argon matrix by Maier and co-workers might be due to $HSiNH_2$−X complexes (X denotes any other species in the system, such as the eliminated N_2). The NH_2 wagging vibration at 938.6 cm^{-1} reported here was not observed by Maier et al. This mode probably was masked by absorptions of the H_3SiN_3 precursor in their experiments. The two N−H stretching modes were too weak to be observed in our experiments.

In good agreement with previous theoretical calculations,[21] the present DFT calculations at the B3LYP/6-311++G(d,p) level predict that the $HSiNH_2$ molecule has a singlet ground state with planar C_s symmetry and is the global minimum on the $SiNH_3$ potential energy surface. As listed in Table 3, the six observed vibrations were calculated at 2001.6, 1602.7, 969.2, 844.2, and 601.9 cm^{-1}. Both the vibrational frequencies and the isotopic frequency shifts matched the observed values very well.

$HGeNH_2$. Similar absorptions at 1793.3, 863.2, 692.8, and 474.0 cm^{-1} can be assigned to the $HGeNH_2$ molecule. The 1793.3 cm^{-1} absorption exhibited no obvious N-15 shift and is due to a Ge−H stretching vibration. The 692.8 cm^{-1} band shifted to 678.4 cm^{-1} with $^{15}NH_3$ and is due to a Ge−N stretching vibration. The bands at 863.2 and 474.0 cm^{-1} exhibited small N-15 shifts and are NH_2 wagging and out-of-plane rocking vibrations, respectively. The $HGeNH_2$ molecule was predicted to have a singlet ground state with planar C_s

symmetry analogous to $HSiNH_2$. As listed in Table 4, the calculated vibrational frequencies and isotopic frequency shifts of the Ge−H stretching, NH_2 wagging, Ge−N stretching, and NH_2 out-of-plane rocking vibrations are in good agreement with the observed values.

SiNH. The absorptions at 3570.8, 1196.9, and 514.9 cm^{-1} that appeared together upon full-arc photolysis are assigned to the SiNH molecule. The 1196.9 cm^{-1} band exhibited a 23.7 cm^{-1} N-15 shift and is due to a Si−N stretching vibration. The 3570.8 cm^{-1} band shifted to 3561.3 cm^{-1} with $^{15}NH_3$ and is a N−H stretching vibration. The 514.9 cm^{-1} band underwent a 2.6 cm^{-1} N-15 shift and is attributed to the SiNH bending vibration. The infrared spectrum of SiNH in solid argon matrix has been previously reported by Ogilivie and Cradock.[18] The three vibrational fundamentals were observed at 3583, 1198, and 523 cm^{-1}, in reasonable agreement with our values. Recent high-resolution infrared emission spectra of SiN−H stretching in the gas phase revealed a value of 3588.4 cm^{-1}.[36] Our DFT calculations predicted that the SiNH molecule has a $^1\Sigma^+$ ground state, in agreement with previous theoretical calculations.[22,23] As listed in Table 3, the calculated vibrational frequencies and relative intensities matched the experimental values.

Reaction Mechanism. Co-condensation of laser-ablated Si or Ge atoms with ammonia in excess argon at 11 K formed $SiNH_3$ and $GeNH_3$ complexes. The absorptions of these complexes increased markedly upon annealing, indicating that ground-state Si or Ge atoms react with NH_3 to form the complexes with no activation energy

$$Si(^3P) + NH_3 \rightarrow SiNH_3(^3A_1) \quad \Delta E = -19.6 \text{ kcal/mol} \quad (1)$$

$$Ge(^3P) + NH_3 \rightarrow GeNH_3(^3A_1) \quad \Delta E = -17.4 \text{ kcal/mol} \quad (2)$$

The $SiNH_3$ and $GeNH_3$ absorptions disappeared upon photolysis at $\lambda > 290$ nm with the emergence of the $HSiNH_2$ and $HGeNH_2$ absorptions, suggesting that the $HSiNH_2$ and $HGeNH_2$ molecules are generated from $SiNH_3$ and $GeNH_3$ via reactions 3 and 4, which were predicted to be exothermic

$$SiNH_3(^3A_1) \rightarrow HSiNH_2(^1A') \quad \Delta E = -46.3 \text{ kcal/mol} \quad (3)$$

$$GeNH_3(^3A_1) \rightarrow HGeNH_2(^1A') \quad \Delta E = -29.8 \text{ kcal/mol} \quad (4)$$

Subsequent full-arc photolysis destroyed the $HSiNH_2$ absorptions and produced the SiNH absorptions. The SiNH molecules are most likely produced by H_2 elimination from the $HSiNH_2$ molecules via reaction 5. In the Ge experiments, the $HGeNH_2$ absorptions were also destroyed upon full-arc photolysis, but no obvious absorptions in the 4000−400 cm^{-1} region were produced. Analogously to Si, the formation of GeNH via H_2 elimination, reaction 6, was predicted to be slightly endothermic. DFT calculations for the $^1\Sigma^+$ ground-state GeNH provided frequencies at 3697.6, 989.1, and 424.1 cm^{-1} with relative intensities of 85:78:464. The most intense bending vibration is probably under 400 cm^{-1}, which is out of our detection range. The N−H stretching and Ge−N stretching vibrations are much weaker and could easily be masked by strong NH_3 or $(NH_3)_n$ absorptions.

$$HSiNH_2(^1A') \rightarrow SiNH(^1\Sigma^+) + H_2 \quad \Delta E = +13.7 \text{ kcal/mol} \quad (5)$$

$$HGeNH_2(^1A') \rightarrow GeNH(^1\Sigma^+) + H_2 \quad \Delta E = +19.6 \text{ kcal/mol} \quad (6)$$

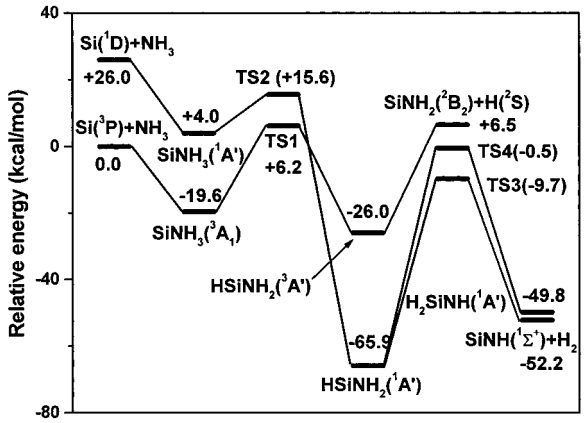

Figure 6. Potential energy surface along the Si + NH_3 reaction path calculated at the B3LYP/6-311++G(d,p) level. Energies are given in kcal/mol and are relative to the reactants $Si(^3P)$ + $NH_3(^1A_1)$.

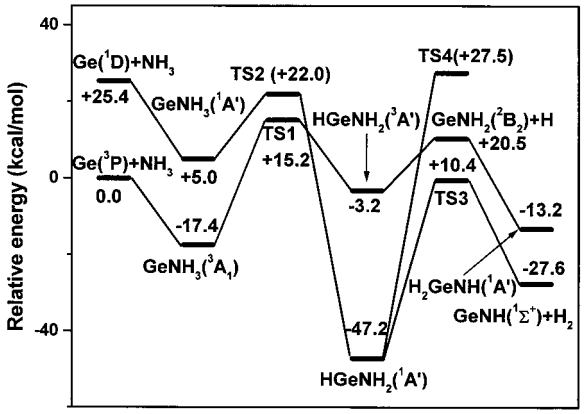

Figure 7. Potential energy surface along the Ge + NH_3 reaction path calculated at the B3LYP/6-311++G(d,p) level. Energies are given in kcal/mol and are relative to the reactants $Ge(^3P)$ + $NH_3(^1A_1)$.

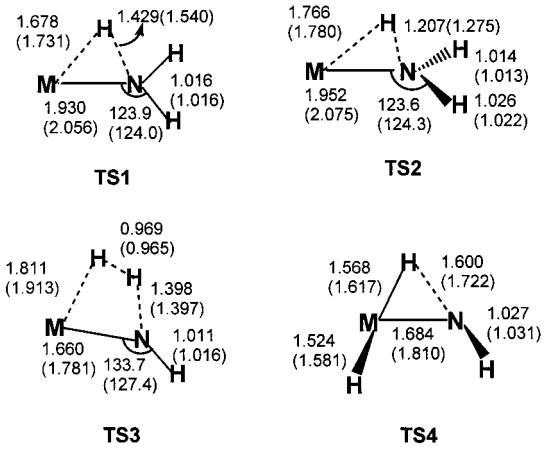

Figure 8. Calculated geometric parameters (bond lengths in angstroms, bond angles in degrees) of the transition states. Values for the Ge reaction system are listed in parentheses.

To obtain a better understanding of the reaction mechanism, potential energy surfaces along the reaction paths were calculated, and the results are shown in Figures 6 and 7, with the optimized transition state structures shown in Figure 8. On both the singlet and triplet potential energy surfaces of the Si + NH_3 reaction, the first step is the formation of the $SiNH_3$ complex; this adduction reaction is exothermic and barrier-free. From the $SiNH_3$ complex, one H atom is passed from N to Si, leading to the $HSiNH_2$ intermediate through transition states TS1 and TS2. As the $SiNH_3$ complex has a triplet ground state whereas the

$HSiNH_2$ has a singlet ground state, there is spin crossing from triplet $SiNH_3$ to singlet $HSiNH_2$. The transition state TS1 lies about 6.2 kcal/mol above the energy of the ground-state reactants, and the energy barrier was estimated to be 25.8 kcal/mol.

From singlet $HSiNH_2$, two reaction paths are possible. One path is H_2 elimination to form SiNH through transition state TS3. Another path is one-hydrogen-atom transfer from nitrogen to the Si center to form H_2SiNH through transition state 4 (TS4). TS3 lies about 9.2 kcal/mol lower in energy than TS4, indicating that the energy barrier for the formation of SiNH is 9.2 kcal/mol lower than that for the formation of H_2SiNH. The isomerization reaction from $HSiNH_2$ to H_2SiNH has been previously studied by Truong and Gordon with ab initio methods.[21] The energy barrier of this isomerization reaction was predicted to be about 78 kcal/mol, 12.6 kcal/mol higher than our DFT value.

Maier and co-workers suggested that $HSiNH_2$ might not be directly transformed into SiNH.[20] They assumed that the reaction proceeded via a H_2SiNH intermediate, which has been observed at 2253, 2175, and 1097 cm^{-1} in solid argon.[20] No H_2SiNH absorptions were observed in our experiments. The present DFT calculations predict that the H_2SiNH molecule has a $^1A'$ ground state and is about 16.1 kcal/mol higher in energy than the $HSiNH_2$ molecule. The calculated potential energy surface also suggests that H_2SiNH is not the intermediate along the reaction path from $HSiNH_2$ to SiNH + H_2.

The Si + NH_3 reaction is quite similar to the Si + H_2O reaction reported previously.[35] Initially, silicon atoms interact with water to form a $SiOH_2$ adduct, which rearranges spontaneously to give HSiOH. When strongly irradiated, the HSiOH intermediate undergoes photolytic decomposition to give silicon monoxide, rather than forming H_2SiO.[37]

As shown in Figure 7, the potential energy surface for the Ge + NH_3 reaction is quite similar to that of the Si + NH_3 reaction. Spin crossing also occurs from the triplet ground-state $GeNH_3$ to the singlet ground-state $HGeNH_2$. The transition state TS1 lies 15.2 kcal/mol higher in energy than the separate reactants, and the energy barrier for this reaction is predicted to be about 32.6 kcal/mol. Two reaction paths starting from singlet $HGeNH_2$ are also possible: one path is the formation of H_2GeNH, and the other is the formation of GeNH + H_2. The energy barrier of the reaction path for the formation of GeNH is 17.1 kcal/mol lower than that of the reaction path for the formation of H_2GeNH.

The photochemical reactions of $HSiNH_2$ and $HGeNH_2$ are distinctly different with those of group 13 metals. The reactions of group 13 metal atoms with NH_3 were reported quite recently,[14] and the $HMNH_2$ molecules (M = Al, Ga, and In) were found to prefer to decompose to form the monovalent MNH_2 molecule upon exposure to broad-band UV−visible light. According to calculations, the $HMNH_2$ molecules (M = Al, Ga, and In) have doublet ground states, whereas the MNH_2 molecules have singlet ground states. Thus, the $HMNH_2 \rightarrow H + MNH_2$ reaction conserves spin. As discussed by the authors, the hydrogen atom expelled in this reaction is able to escape from the matrix cage because of its small size. For comparison, we calculated part of the potential energy surface of the Al + NH_3 reaction at the B3LYP/6-311++G(d,p) level, and the results are shown in Figure 9. From doublet $HAlNH_2$, the loss of one H atom to form $AlNH_2$ proceeds without a transition state. This process was predicted to be endothermic by about 40.9 kcal/mol. The $HAlNH_2 \rightarrow AlNH + H_2$ reaction was calculated to be endothermic by about 44.0 kcal/mol. Although

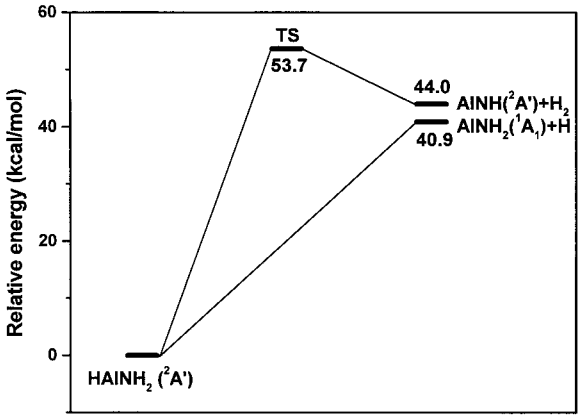

Figure 9. Potential energy surface following the reaction paths from $HAlNH_2$ leading to $AlNH_2$ + H and AlNH + H_2. Energies are given in kcal/mol and are relative to $^2A'$ $HAlNH_2$ ($HAlNH_2$, planar C_s symmetry, H−Al = 1.604 Å, Al−N = 1.794 Å, N−H = 1.010/1.013 Å, ∠HAlN = 115.7°, ∠AlNH = 125.6/124.5°; $AlNH_2$, planar C_{2v} symmetry, Al−N = 1.820 Å, N−H = 1.015 Å, ∠AlNH = 125.8°; AlNH, bent C_s symmetry, Al−N = 1.761 Å, N−H = 1.019 Å, ∠AlNH = 134.7°).

the endothermicity for this H_2-elimination reaction is only slightly higher than that of the $HAlNH_2 \rightarrow AlNH_2 + H$ reaction, the H_2 elimination reaction proceeds via a transition state with an energy barrier of 53.7 kcal/mol. Apparently, the formation of $AlNH_2$ is energetically favored over the formation of AlNH. The situation was reversed in the case of Si. As shown in Figure 6, the $SiNH_2$ molecule was predicted to have a $^2B_2$ ground state, and the formation of H + $SiNH_2$ from singlet ground-state $HSiNH_2$ is a spin-forbidden process that is energetically unfavorable. No evidence was found for the $SiNH_2$ molecule in our experiments.

The photochemical reactions of $HMNH_2$ (M denotes main group metal atoms including Al, Ga, In, Si, and Ge) are also quite different from those of early transition metal atoms. Recent investigations in our laboratory showed that, for Ti and V group metals, the major photochemical reaction channel of the $HMNH_2$ molecule is the formation of H_2MNH.[38]

5. Conclusions

The reactions between Si and Ge atoms and NH_3 molecules were investigated using the matrix-isolation technique. Various reaction intermediates and products were produced and trapped via thermal and photochemical reactions in solid argon and characterized by infrared spectra and density functional theoretical calculations. Silicon and germanium atoms reacted with NH_3 to form the $SiNH_3$ and $GeNH_3$ complexes spontaneously upon annealing. Mercury arc photolysis with a 290-nm long-wavelength pass filter induced isomerization of the complexes to form the inserted $HSiNH_2$ and $HGeNH_2$ molecules. The $HSiNH_2$ molecule further decomposed to SiNH + H_2 upon full-arc irradiation (250−580 nm). The potential energy surfaces along the reaction path leading to the observed products were calculated to assist in interpreting the reaction mechanism.

The photochemical reaction of $HSiNH_2$ is distinctly different from those of group 13 metals. Upon exposure to broad-band UV−visible light, the $HMNH_2$ molecules (M = Al, Ga, and In) prefer to lose one H atom to form the monovalent MNH_2 molecule, but H_2 elimination dominates the $HSiNH_2$ reaction. The chemistries of $HMNH_2$ (M = Al, Ga, and In) and $HSiNH_2$ differ so greatly because Si has two valence p electrons whereas group 13 metals has only one.

Acknowledgment. We acknowledge support for this research from NSFC (Grant 20003003 and 20125033) and the Chinese NKBRSF.

References and Notes

(1) See, for example: Fattal, E.; Radeke, M. R.; Reynolds, G.; Carter, E. A. *J. Phys. Chem. B* **1997**, *101*, 8658 and references therein.

(2) Colaianni, M. L.; Chen, P. J.; Yates, J. T., Jr. *J. Chem. Phys*. **1992**, *96*, 7826. Stober, J.; Eisenhut, R.; Rangelor, G.; Fauster, T. *Surf. Sci*. **1994**, *321*, 111.

(3) Bower, J. E.; Jarrold, M. F. *J. Chem. Phys*. **1992**, *97*, 8312. Patterson, C. H.; Messmer, R. P. *Phys. Rev. B* **1990**, *42*, 7530.

(4) Ratcliff, L.; Holme, T. *J. Phys. Chem. A* **1998**, *102*, 9531.

(5) See, for example: Fredin, L.; Hauge, R. H.; Kafafi, Z. H.; Margrave, J. L. *J. Chem. Phys.* **1985**, *82*, 3542. Chertihin, G. V.; Andrews, L. *J. Am. Chem. Soc*. **1994**, *116*, 8322. Pullumbi, P.; Bouteiller, Y.; Manceron, L.; Mijoule, C. *Chem. Phys*. **1994**, *185*, 25.

(6) See, for example: Chertihin, G. V.; Saffel, W.; Yustein, J. T.; Andrews, L.; Neurock, M.; Ricca, A.; Bauschlicher, C. W., Jr. *J. Phys. Chem.* **1996**, *100*, 5261. Chertihin, G. V.; Andrews, L. *J. Phys. Chem.* **1995**, *99*, 6356.

(7) See, for example: Kauffman, J. W.; Hauge, R. H.; Margrave, J. L. *J. Phys. Chem*. **1985**, *89*, 3541; **1985**, *89*, 3547.

(8) See, for example: Suzer, S.; Andrews, L. *J. Am. Chem. Soc*. **1987**, *109*, 300. Thompson, C. A.; Andrews, L.; Martin, J. M. L.; El-Yazal, J. *J. Phys. Chem*. **1995**, *99*, 13839.

(9) Kauffman, J. W.; Hauge, R. H.; Margrave, J. L. *High Temp. Sci*. **1984**, *17*, 237. Szczepanski, J.; Szczesniak, M.; Vala, M. *Chem. Phys. Lett*. **1989**, *162*, 123.

(10) Ball, D. W.; Hauge, R. H.; Margrave, J. L. *High Temp. Sci*. **1988**, *25*, 95.

(11) Ball, D. W.; Hauge, R. H.; Margrave, J. L. *Inorg. Chem*. **1989**, *28*, 1599.

(12) Howard, J. A.; Joly, H. A.; Edwards, P. P.; Singer, R. J.; Logan, D. E. *J. Am. Chem. Soc*. **1992**, *114*, 474.

(13) Lanzisera, D. V.; Andrews, L. *J. Phys. Chem. A* **1997**, *101*, 5082.

(14) Himmel, H. J.; Downs, A. J.; Greene, T. M. *J. Am. Chem. Soc*. **2000**, *122*, 9793.

(15) Zhang, L. N.; Dong, J.; Zhou, M. F. *J. Phys. Chem. A* **2000**, *104*, 8882. Zhou, M. F.; Zhang, L. N.; Shao, L. M.; Wang, W. N.; Fan, K. N.; Qin, Q. Z. *J. Phys. Chem. A* **2001**, *105*, 5801.

(16) Zhou, M. F.; Zhang, L. N.; Dong, J.; Qin, Q. Z. *J. Am. Chem. Soc.* **2000**, *122*, 10680. Zhou, M. F.; Dong, J.; Zhang, L. N.; Qin, Q. Z. *J. Am. Chem. Soc*. **2001**, *123*, 135.

(17) Shao, L. M.; Zhang, L. N.; Lu, H., Chen, M. H.; Zhou, M. F. *Chem. Phys. Lett*. **2001**, *343*, 178.

(18) Ogilvie, J. F.; Cradock, S. *J. Chem. Soc., Chem. Commun.* **1966**, 364.

(19) Maier, G.; Glatthaar, J.; Reisenauer, H. P. *Chem. Ber*. **1989**, *122*, 2403.

(20) Maier, G.; Glatthaar, J. *Angew. Chem., Int. Ed. Engl*. **1994**, *33*, 473.

(21) Truong, T. N.; Gordon, M. S. *J. Am. Chem. Soc*. **1986**, *108*, 1775.

(22) Melius, C. F.; Ho, P. *J. Phys. Chem*. **1991**, *95*, 1410.

(23) Jursic, B. S. *THEOCHEM* **1999**, *460*, 11. Kwon, O.; Kwon, Y. *THEOCHEM* **1999**, *460*, 213.

(24) Chen, M. H.; Wang, X. F.; Zhang, L. N.; Yu, M.; Qin, Q. Z. *Chem. Phys*. **1999**, *242*, 81.

(25) Frisch, M. J.; Trucks, G. W.; Schlegel, H. B.; Scuseria, G. E.; Robb, M. A.; Cheeseman, J. R.; Zakrzewski, V. G.; Montgomery, J. A., Jr.; Stratmann, R. E.; Burant, J. C.; Dapprich, S.; Millam, J. M.; Daniels, A. D.; Kudin, K. N.; Strain, M. C.; Farkas, O.; Tomasi, J.; Barone, V.; Cossi, M.; Cammi, R.; Mennucci, B.; Pomelli, C.; Adamo, C.; Clifford, S.; Ochterski, J.; Petersson, G. A.; Ayala, P. Y.; Cui, Q.; Morokuma, K.; Malick, D. K.; Rabuck, A. D.; Raghavachari, K.; Foresman, J. B.; Cioslowski, J.; Ortiz, J. V.; Baboul, A. G.; Stefanov, B. B.; Liu, G.; Liashenko, A.; Piskorz, P.; Komaromi, I.; Gomperts, R.; Martin, R. L.; Fox, D. J.; Keith, T.; Al-Laham, M. A.; Peng, C. Y.; Nanayakkara, A.; Gonzalez, C.; Challacombe, M.; Gill, P. M. W.; Johnson, B.; Chen, W.; Wong, M. W.; Andres, J. L.; Gonzalez, C.; Head-Gordon, M.; Replogle, E. S.; Pople, J. A. *Gaussian 98*, revision A.7; Gaussian, Inc.: Pittsburgh, PA, 1998.

(26) Becke, A. D. *J. Chem. Phys.* **1993**, *98*, 5648.

(27) Lee, C.; Yang, E.; Parr, R. G. *Phys. Rev. B* **1988**, *37*, 785.

(28) McLean, A. D.; Chandler, G. S. *J. Chem. Phys*. **1980**, *72*, 5639. Krishnan, R.; Binkley, J. S.; Seeger, R.; Pople, J. A. *J. Chem. Phys*. **1980**, *72*, 650.

(29) Wachter, J. H. *J. Chem. Phys.* **1970**, *52*, 1033. Hay, P. J. *J. Chem. Phys*. **1977**, *66*, 4377.

(30) Head-Gordon, M.; Pople, J. A.; Frisch, M. *Chem. Phys. Lett*. **1988**, *153*, 503.

(31) Suzer, S.; Andrews, L. *J. Chem. Phys.* **1987**, *87*, 5131.

(32) Nelander, B.; Nord, L. *J. Phys. Chem*. **1982**, *86*, 4375.

(33) Zhou, M. F.; Zhang, L. N.; Lu, H.; Shao, L. M.; Chen, M. H. *J. Mol. Struct*., in press.

(34) Khabashesku, V. N.; Kudin, K. N.; Margrave, J. L.; Fredin, L. *J. Organmet. Chem.* **2000**, *595*, 248.

(35) Ismail, Z. K.; Hauge, R. H.; Fredin, L.; Kauffman, J. W.; Margrave, J. L. *J. Chem. Phys*. **1982**, *77*, 1617.

(36) Elhanine, M.; Farrenq, R.; Guelachvili, G. *J. Chem. Phys*. **1991**, *94*, 2529.

(37) Withnall, R.; Andrews, L. *J. Phys. Chem*. **1985**, *89*, 3261.

(38) Zhou, M. F.; Chen, M. H.; Lu, H., to be published.